PNAS RESEARCH ARTICLE | ENGINEERING

Three-chamber electrochemical reactor for selective lithium extraction from brine

Yuge Feng[a], Yoon Park[a], Shaoyun Hao[a], Zhiwei Fang[a], Tanguy Terlier[b], Xiao Zhang[a], Chang Qiu[a], Shoukun Zhang[a], Fengyang Chen[a], Peng Zhu[a], Quan Nguyen[a], Haotian Wang[a,c,d,e,1], and Sibani Lisa Biswal[a,c,e,1]

Affiliations are included on p. 8.

Edited by Yi Cui, Stanford University, Stanford, CA; received May 20, 2024; accepted October 4, 2024

Efficient lithium recovery from geothermal brines is crucial for the battery industry. Current electrochemical separation methods struggle with the simultaneous presence of Na^+, K^+, Mg^{2+}, and Ca^{2+} because these cations are similar to Li^+, making it challenging to separate effectively. We address these challenges with a three-chamber reactor featuring a polymer porous solid electrolyte in the middle layer. This design improves the transference number of Li^+ (t_{Li+}) by 2.1 times compared to the two-chamber reactor and also reduces the chlorine evolution reaction, a common side reaction in electrochemical lithium extraction, to only 6.4% in Faradaic Efficiency. Employing a lithium-ion conductive glass ceramic (LICGC) membrane, the reactor achieved high t_{Li+} of 97.5% in LiOH production from simulated brine, while the concentrations of Na^+ K^+, Mg^{2+}, and Ca^{2+} are below the detection limit. Electrochemical experiments and surface analysis elucidated the cation transport mechanism, highlighting the impact of Na^+ on Li^+ migration at the LICGC interface.

lithium extraction | electrochemical reactor | lithium selectivity

Lithium is an essential and valuable element used for energy production, energy storage, glass production, and pharmaceuticals (1–5). Since 2015, the demand for lithium has increased sharply by around 41.6%, reaching 0.049 million tons in 2020. Projections estimate this demand to reach around 0.77 million tons in 2050, leading to potential supply issues (6, 7) However, conventional lithium mining from ore is energy-intensive, environmentally destructive, and faces diminishing reserves of lithium-rich ore (8). Seawater contains substantial lithium reserves, but its low lithium concentration (0.17 ppm) limits effective collection (9). Therefore, Geothermal brines, with high lithium concentrations (up to 3800 mg/L), have become an attractive alternative source of lithium (10, 11). Yet, the presence of coexisting cations, such as Na^+, K^+, Mg^{2+}, and Ca^{2+}, makes separation difficult. Currently, industrial recovery of lithium from brines relies on a solar evaporation-precipitation method, known for cost-effectiveness and energy efficiency. However, this method is time-consuming (2 to 18 mo), requires a significant land footprint, and its yield is highly dependent on the local weather conditions (3, 12, 13). Other traditional lithium extraction technologies include adsorption (14, 15), ion exchange (16), and solvent extraction (17, 18). These methods are faster but are limited by costs, low selectivity, and the risk of environmental pollution. Consequently, there remains an urgent need to establish a more sustainable and efficient approach for lithium extraction from geothermal brines.

One promising new direction is the application of electrochemical separation, which can extract lithium using renewable electricity. Through the careful design of an electrochemical reactor, lithium extraction can be coupled with electrochemical reactions to produce the desired product; and with ion-selective materials, Li^+ can be separated with high selectivity. Electrodialysis (19–22) is a common electrochemical lithium recovery strategy, but requires several chambers separated by ion-selective cation exchange membranes (CEMs) and anion exchange membranes (AEM). Further, the process typically results in a chlorine evolution reaction (CER) due to the high Cl^- concentration in the brine. Last, additional treatment is sometimes necessary to convert LiCl to the desired battery feedstocks, such as Li_2CO_3 or LiOH [note: LiOH is more favored because of its lower melting point (23)]. Battery-based technologies (24–28) are also widely reported for lithium extraction. These systems employ the faradaic intercalation between electrodes and have demonstrated high selectivity for Li^+ over Na^+(on the order of 10^4), but generally involve two steps (capture and release) and are limited by the

Significance

This study addresses a critical challenge in developing domestic lithium resources from geothermal brines: selectively extracting lithium from chemically similar cations like sodium. We utilize a three-chamber electrochemical reactor coupled with a highly lithium-selective membrane, enabling efficient and environmentally sustainable extraction of high-purity lithium. Our electrochemical reactor enhances lithium selectivity compared to conventional methods by decoupling lithium extraction from counterion transport. This innovation broadens the applicability to various lithium-containing feedstocks. Moreover, insights into cation transport mechanisms gained from this work advance the design of selective membranes for lithium separation. By improving lithium extraction efficiency while reducing environmental impact, our study makes a significant contribution toward establishing a robust domestic supply of this critical energy material for sustainable energy solutions.

This article is a PNAS Direct Submission.

[1]To whom correspondence may be addressed. Email: htwang@rice.edu or biswal@rice.edu.

This article contains supporting information online at https://www.pnas.org/lookup/suppl/doi:10.1073/pnas.2410033121/-/DCSupplemental.

Published November 11, 2024.

electrode Li^+ storage capacity. More recently, a two-chamber reactor has been reported with high selectivity using the lithium-ion conductive glass ceramic (LICGC) membrane (5). However, the two-chamber design requires the brine to flow on the anode side, which results in the undesirable side reaction of CER. In addition, this technique involves a flammable organic solvent as catholyte, and the final product is lithium metal. There is a need for a continuous separation process that directly yields LiOH as the final product, while minimizing the side reaction of CER on the anode side, and ensuring high Li^+ selectivity on the cathode side.

In this work, a three-chamber reactor for direct and continuous electrochemical lithium recovery was designed. The three-chamber cell separates the brines from the anode side with a CEM to suppress CER and improves the t_{Li+} by buffering the H^+ concentration with a middle layer filled with polymer porous solid electrolyte (PSE). Utilizing a LICGC membrane ensures selective extraction of Li^+ from the coexisting cations, achieving a remarkable Li^+ transference number (t_{Li+}) of 97.5%.

Results and Discussion

Design of the Three-Chamber Cell Reactor. Conventional electrochemical reactors for lithium recovery (5, 21) commonly adopt the two-chamber configuration, such as an H-cell or a membrane electrode assembly. In a two-chamber reactor, as mentioned in the introduction and depicted in Fig. 1*A*, brines flow on the anode side, and products ($LiCl/Li_2CO_3$/metallic Li) are collected on the cathode side. However, due to the high Cl^- concentration in brines, CER competes with oxygen evolution reaction (OER) on the anode side, generating poisonous chlorine gas and hypochlorous acid that can lead to electrode and membrane degradation and can be also hazardous to human health and environments. In addition, protons generated by the OER create an acidic environment on the membrane surface. Consequently, protons will compete with Li^+ (and Na^+), leading to low Li^+ (and Na^+)/H^+ selectivity, and the dissipation of energy. Furthermore, as shown in Fig. 1*C*, 79.7% of the electricity is wasted transporting protons.

To minimize CER and increase t_{Li+}, we designed a three-chamber electrochemical reactor for direct lithium recovery to LiOH from simulated geothermal brines (1.0 M NaCl, 0.05 M LiCl). The three chambers were separated by two CEMs, and PSE was added to the middle chamber to promote ion transportation and to lower the resistance. Similar designs were previously reported for a wide range of electrochemical applications, including CO_2 reduction reactions to pure liquid products (29), oxygen reduction to electrolyte-free hydrogen peroxide (30), as well as electrochemical carbon capture (31). As depicted in Fig. 1*B*, the simulated brine containing LiCl and NaCl flowed into the middle chamber, while deionized (DI) water flowed in both the anode and cathode. Since the anode chamber was separated from the middle layer by a CEM, the concentration of Cl^- in the anode chamber was significantly lower than that in the two-chamber configurations. Therefore, in the three-chamber configuration, CER is reduced. As shown in Fig. 1*C*, the chlorine/hypochlorous Faradaic Efficiency (FE) for the three-chamber cell was only 6.4% compared to 14.3% for the two-chamber device under 100 mA (active area: 4 cm^2) (please refer to the Experimental Methods and *SI Appendix*, Fig. S19 for details regarding the titration method), making the reactor more manageable to handle and more environmentally friendly. In addition, the protons generated from OER were effectively diluted and buffered inside the middle layer before they reached the membrane interface. Therefore, with a lower concentration of H^+ at the membrane interface, higher Li^+ and Na^+ transference number (71.0%) was achieved in the three-chamber configuration compared to the two-chamber configuration (20.3%), as shown in Fig. 1*C*. However, both the PSE and the Nafion were not selective for Li^+ over Na^+. Although FE_{Li+} was improved by 2.1 times using our three-chamber reactor, NaOH was still the dominant product. Higher FE_{Li+} required Li^+/Na^+ selective membranes.

Although some membranes were reported to be selective for Li^+ over Ca^{2+}, Mg^{2+}, and K^+ (22, 32, 33), separating of Li^+ from Na^+ using membrane remained challenging (34–39). In pursuit of a high Li^+/Na^+ selectivity, we opted for the LICGCs membrane purchased from the Ohara Corporation ($Li_{1+x+y}Al_xTi_{2-x}Si_yP_{3-y}O_{12}$) with a lithium conductivity of 4×10^{-4} S/cm. The LICGCs have been utilized in various applications for Li^+ conduction (5, 21, 40–47). An obstacle encountered when using the LICGC membrane was its poor mechanical strength (46, 48). To protect the membrane while minimizing the contact resistance, we carved grooves of specific depths onto the cathode metal plate and the middle-chamber holder and placed two rubber O-rings to secure and protect the ceramic membrane, as illustrated in Fig. 2*A*. The functionalized PSE with sulfonate groups in the middle layer guaranteed efficient Li^+ and Na^+ conduction, while only Li^+ could be transported through the LICGC membrane, producing LiOH as the final product. We conducted systematic electrochemical lithium recovery studies with the LICGC and the modified three-chamber reactor.

Electrochemical Lithium Recovery Performance. A simulated brine with an initial Li: Na ratio of 1:100 (0.01 M LiCl, 1.0 M NaCl) was used to test electrochemical lithium recovery. The Li^+ and Na^+ concentrations in the catholyte were tested using ionic chromatography (IC; see *SI Appendix*, Fig. S15 for IC calibration), and the t_{Li+} was calculated based on the Li^+ concentration measured in the catholyte. The t_{Li+} was relatively stable during the recovery, with an average of 97.5 ± 3.2%. The concentrations of Na^+ were below the detection limit IC (*SI Appendix*, Fig. S14), indicating a Li^+/Na^+ selectivity factor over 2.5×10^3 (Fig. 2*B*). The cell voltage starts at a low value of 1.4 V; however, we noticed an increase of above 1.0 V (Fig. 2*B* and *SI Appendix*, Fig. S4*B*) during the 150-min of continuous operation.

Control experiments were conducted to better understand the lithium extraction process and to determine the reason for the increase in cell voltage. A 0.50 M LiCl solution was first flowed in the middle layer to evaluate the intrinsic stability of the LICGCs. When applying a current of 0.2 mA (active area: 4 cm^2, 50 $\mu A/cm^2$), the cell voltage remained stable at 1.1 V for over 100 h (Fig. 2*C*). This result demonstrated that given a sufficient Li^+ source, the membrane exhibited prolonged stability. The stable cell voltage also reflected a steady Li^+ transport within the system. To determine whether the Li^+ concentration in the simulated brine (0.01 M) was adequate for the applied current, we varied the middle layer Li^+ concentration from 1.00 M to 0.05 M and 0.01 M. As shown in Fig. 2*D*, cell voltages were higher for lower Li^+ concentrations, which can be explained by lower ionic conductivity. Cell voltages were stable for all three concentration scenarios, and t_{Li+} remained high for all LiCl concentrations

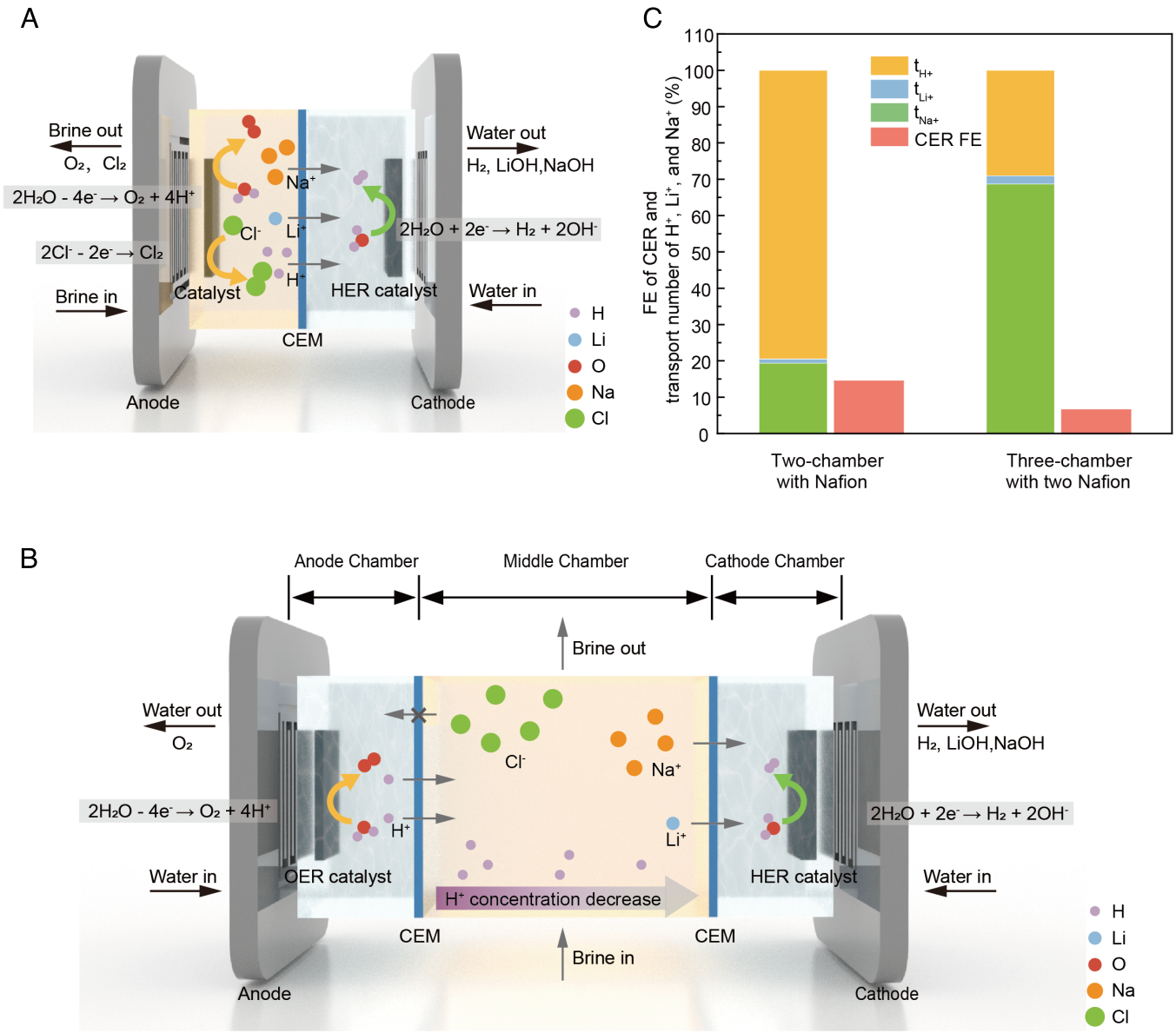

Fig. 1. Schematic and FE and transference number comparison between the two-chamber and three-chamber reactors. (*A*) Scheme of a two-chamber reactor, where brine flows in the anode (*Right*) chamber, producing O_2 and Cl_2. (*B*) Scheme of a three-chamber reactor, where brine flows in the *Middle* chamber, water flows in both anode and cathode chamber, and the three chambers are separated by two CEMs. (*C*) Comparison of the CER FE and the transference number of Li^+, Na^+ for the two-chamber and the three-chamber cell. This experiment is conducted using simulated brines (1.0 M NaCl, 0.05 M LiCl), under 25 mA/cm^2 (4 cm^2).

(*SI Appendix*, Fig. S2*B*), indicating that 0.01 M of Li^+ was sufficient to supply the cell current of 0.2 mA.

The above results showed that the three-chamber system with the LICGC is stable with only Li^+ in the middle layer, suggesting ease of Li^+ transport through the middle layer and LICGC membrane. Thus, we hypothesized that Na^+ cannot transport through the LICGC membrane and will hinder Li^+ transport, leading to increased cell voltage. Therefore, in the subsequent control experiment, Na^+ was introduced into the system. The middle layer fluid underwent alternation between 1.00 M LiCl and 1.00 M NaCl, as visually depicted in Fig. 2*E*. Upon transitioning from the LiCl solution to the NaCl solution, a conspicuous surge in cell voltage from 1.2 V to 10.0 V occurred within 20 min. This result indicated that when LICGC released Li^+ to the catholyte, it absorbed cations from the middle layer. Although Li^+ readily transports from the middle layer to the membrane, Na^+ cannot; thus, when switching to 1.00 M of NaCl in the middle layer, there is a lack of mobile ions for the applied current (0.2 mA, 50 μA/cm^2). Consequently, the cell voltage increased sharply and resulted in cell failure, which supports the first part of our hypothesis that Na^+ cannot flow through the LICGC membrane.

Subsequent reversion to 1.00 M LiCl (illustrated by the dark blue curve in Fig. 2*E*) resulted in the restoration of the cell voltage to 2.0 V. However, it did not recover to the original 1.2 V, suggesting that irreversible changes occurred on the membrane's surface after the NaCl flow. We further hypothesized that Na^+ can also be adsorbed onto the membrane surface with a higher energy barrier compared to Li^+; however, since Na^+ cannot transport through the membrane, it blocks Li^+ transport. To

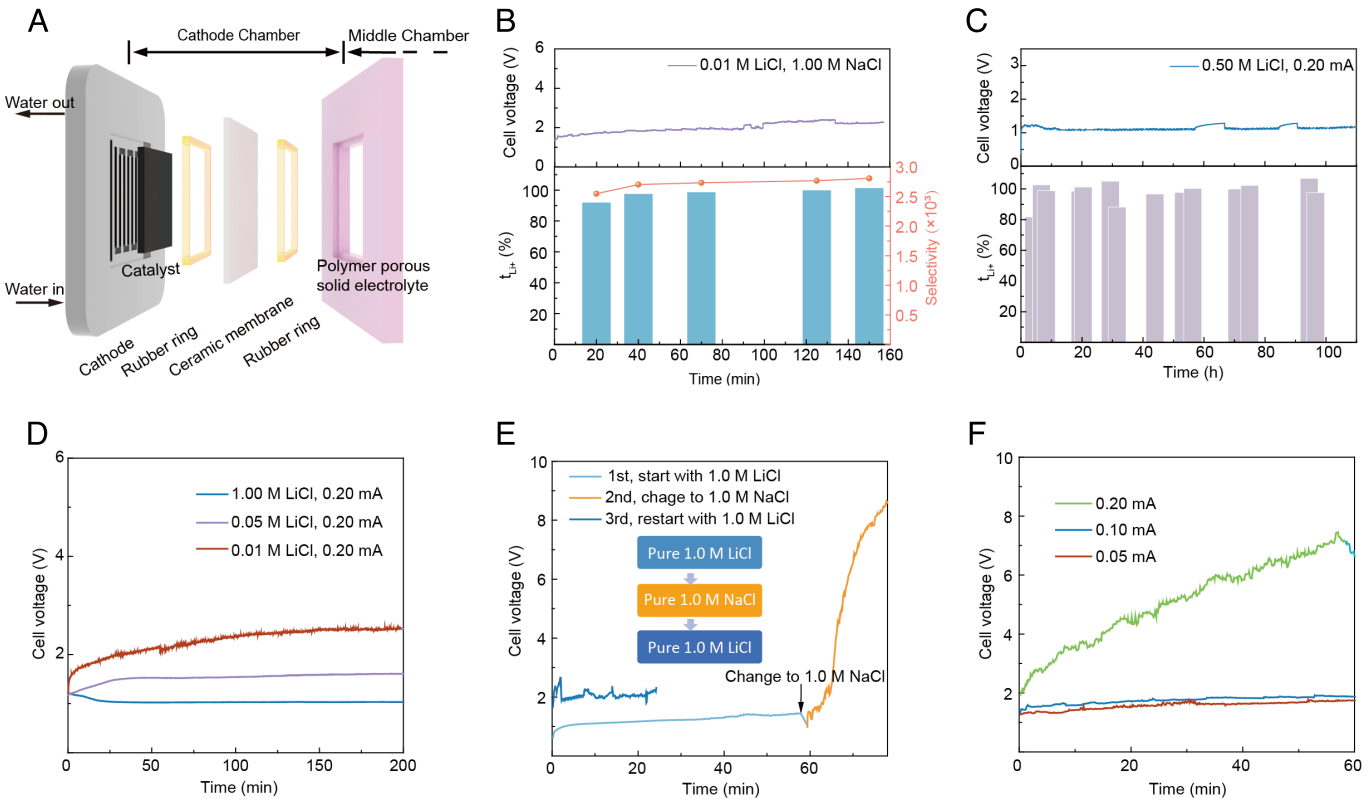

Fig. 2. Schematic and electrochemical performances of the three-chamber PSE reactor with LICGC. (*A*) Scheme of the *Middle* chamber and the cathode chamber, where the *Middle* chamber was filled with PSE, the LICGC membrane was held by two rubber rings that enabled soft contact, and a commercial Pt/C electrode was employed as the cathode catalyst to drive the HER. (*B*) Cell voltage (purple curve), t_{Li+}, and Li^+/Na^+ selectivity for lithium recovery from a simulated brine (1.00 M NaCl, 0.01 M LiCl) under 0.1 mA (25 μA/cm^2). (*C*) Cell voltage and t_{Li+} for lithium extraction from 0.50 M LiCl solution in the *Middle* layer, under 0.2 mA (50 μA/cm2). (*D*) Cell voltages of lithium extraction from different concentrations of LiCl (0.01 M, 0.05 M, 1.00 M) under 0.2 mA. (*E*) Cell voltages during specific operational steps: Step 1 involved operation at 0.2 mA with 1.00 M LiCl in the *Middle* layer for 60 min (depicted by the light blue curve); Step 2 transitioned to 1.00 M NaCl for 20 min (depicted by the orange curve); Step 3 returned to flow with 1.00 M LiCl in the *Middle* layer for 30 min without applied current, followed by a restart at 0.2 mA (depicted by the dark blue curve). (*F*) Cell voltages for lithium extraction from simulated brine (1:100) under 0.20 mA, 0.10 mA, and 0.05 mA (4 cm^2).

verify our hypothesis, different currents (0.2 mA, 0.10 mA, and 0.05 mA) were applied to the system with simulated brine (1 LiCl:100 NaCl ratio) flowing in the middle layer for the final control experiments. As shown in Fig. 2*F*, under 0.20 mA, the cell voltage increased rapidly from 1.9 V to 6.9 V in an hour but was more stable under lower currents (while t_{Li+} remained at over 95%, *SI Appendix*, Fig. S2*C*), suggesting that the membrane is more stable at lower applied currents. These results were consistent with our hypothesis that Na^+ has a higher energy barrier to be adsorbed onto the membrane and is more likely to be adsorbed on the surface of the ceramic under a higher current (electric field). On the contrary, if the reaction is operated under lower currents, less Na^+ will be trapped on the ceramic surface, which enables more efficient Li^+ transport.

Membrane Characterization. The Time-of-Flight Secondary Ion Mass Spectrometry (TOF-SIMS) analysis was performed to map the lithium and sodium distribution at the surface and analyze the elemental composition along the cross-section of the LICGC membrane. Fig. 3*C* showed the total normalized sodium intensity proportion (based on a 10 mm × 10 mm sample area on the surface of the membrane facing the middle layer) on the membrane surface under different conditions: Membrane 1: 0.1 mA 60 min; Membrane 2: 0.2 mA 60 min; Membrane 3: 0.1 mA 150 min (active area 4 cm^2). All three membranes were washed by flowing DI water for 2 min after the reactions. As expected, Membrane 1 had the least sodium (6.35%), followed by Membrane 3 (9.98%), and then Membrane 2 (10.60%). The results suggested less Na^+ on the LICGC surface for a lower current, which also agreed with our hypothesis that a higher current leads to more severe Na^+ fouling. In addition, when constant current was applied, more Na^+ fouling was found for longer operation times.

Fig. 3 *A* and *B* compare the normalized intensity distribution along the depth of the membrane before and after applying current (0.1 mA for 1 h, then the membrane was washed in flowing DI water for 2 min before the characterization). The lithium concentration was the highest at the membrane interface and decreased to a stable value for both the postreaction and the pristine membrane, which is an intrinsic property of the LICGC membrane, likely a result of the manufacturing process. The Li^+ concentration in the membrane was slightly higher after applying current (1.4%) than before applying current (0.8%). The relative intensity proportion of Ti^+, Si^+, and Al^+ ions in the postreaction membrane was lower, which can be explained by the higher Li^+ and Na^+ ion intensity and the subtle intrinsic differences between the two ceramic membranes. The prereaction membrane did not exhibit any observable signal of sodium. For the postreaction membrane, the Na^+ normalized intensity was the highest (9.8%) at around 1 nm and diminished to 0% at approximately 2 nm. At a current of 0.1 mA, it is evident that Na^+ penetration in the membrane was negligible, with

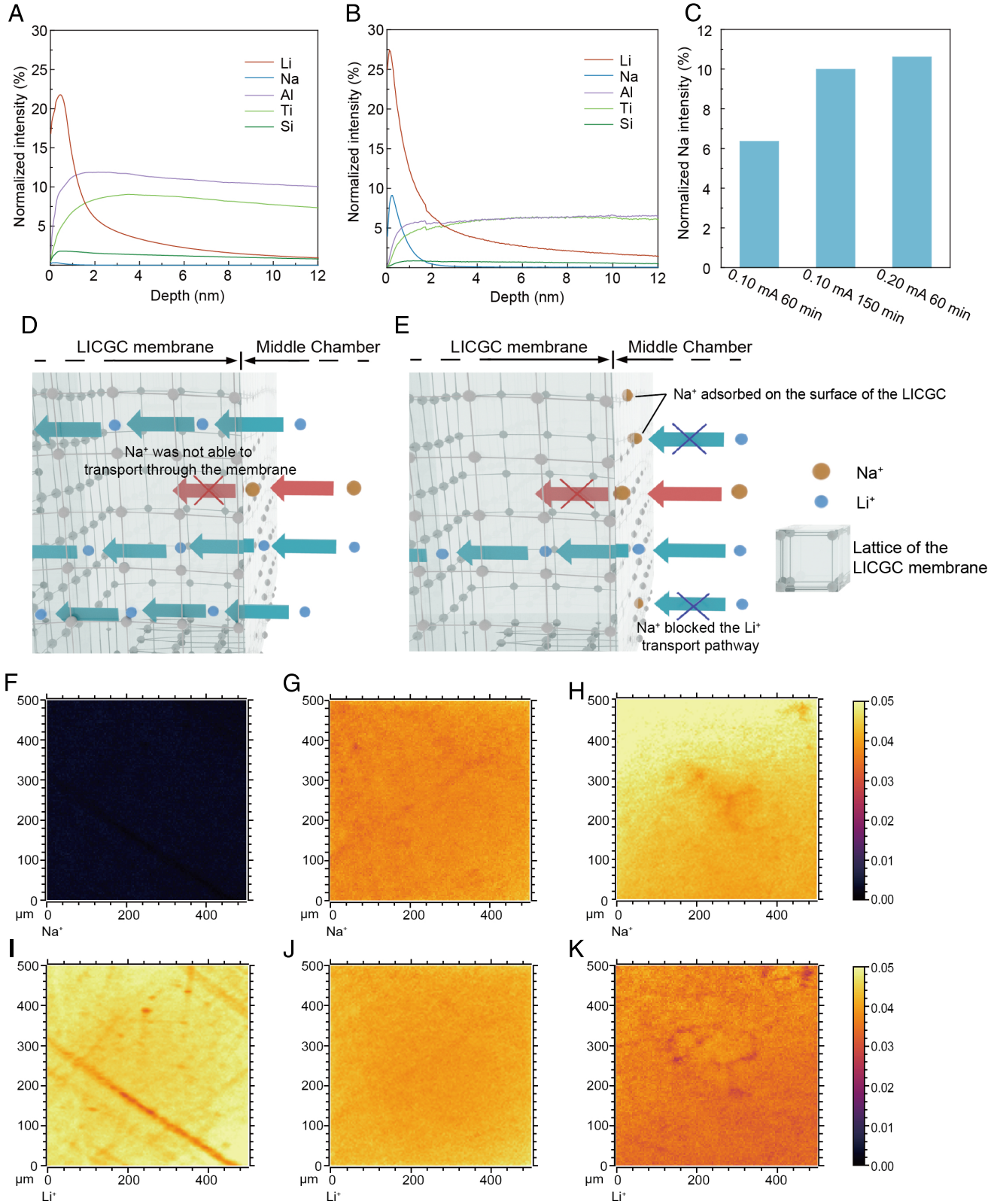

Fig. 3. TOF-SIMS characterization. TOF-SIMS depth profiles of different elemental ions from the surface (facing *Middle* layer) of the (*A*) prereaction and (*B*) postreaction of the LICGC membrane. (*C*) Average TOF-SIMS intensity (over a 10 mm × 10 mm area) of Na^+ on the ceramic surface (facing *Middle* layer) after 0.1 mA 60 min, 0.1 mA 150 min, and 0.2 mA 60 min of operation. Scheme of Li^+ transport at the interface of the *Middle* layer and the LICGC membrane (*D*) at the beginning, when Li^+ transport occurs easily through the membrane and the cell voltage is low; and (*E*) after some time, when Na^+ on the membrane surface blocks the transport of Li^+. Normalized Na^+ intensity on the surface (facing the *Middle* layer) of (*F*) the pristine membrane; (*G*) Membrane 1; and (*H*) Membrane 2. Normalized Li^+ intensity on the surface (facing *Middle* layer) of (*I*) the pristine membrane; (*J*) Membrane 1; and (*K*) Membrane 2. The dark lines are scratches on the membrane created by tweezers during handling.

Na^+ reaching only 0.001% of the thickness of the membrane, and this is also supported by the absence of sodium in the catholyte.

TOF-SIMS intensity patterns of Li^+ and Na^+ for the prereaction membrane, Membrane 1 (after 0.1 mA 60 min), and Membrane 2 (after 0.2 mA 60 min) are shown in Fig. 3 *F–K*. Uniform distributions of Li^+ and Na^+ were observed on all of them. Fig. 3 *F–J* illustrates a minimal Na signal in the pristine membrane, a slightly higher signal in Membrane 1, and a significantly higher signal in Membrane 2. In contrast, the normalized Li signal was highest in the pristine membrane, slightly lower in Membrane 1, and significantly reduced in Membrane 2, as shown in Fig. 3 *G–K*.

The TOF-SIMS results confirmed our hypothesis that, in addition to Li^+ ions, Na^+ ions were also adsorbed onto the membrane surface. However, the adsorbed Na^+ ions were unable to permeate through the membrane or be washed away by water. Thus, Na^+ remained trapped at the membrane surface, impeding the transport of Li^+ through the membrane. Given that Na^+ exhibited a higher energy barrier than Li^+ for adsorption onto the membrane surface, this phenomenon became more pronounced at higher currents. To summarize, the results from TOF-SIMS characterizations and electrochemical experiments aligned well. These collective findings substantiate our hypothesis that Na^+ adversely affects the transport of Li^+ by irreversible adsorbing onto the membrane and obstructing the transport of Li^+ (as schematically illustrated in Fig. 3 *D* and *E*). Note that the LICGC membranes can be regenerated partially by operating with LiCl (1.00 M) solution in the middle layer and a pulse-rest method can also slightly expedite the regeneration process, as shown in *SI Appendix*, Fig. S3.

Electrochemical Performance in the Presence of Coexisting Cations Beyond Na^+. In addition to Na^+, K^+, Mg^{2+}, and Ca^{2+} also coexist with Li^+ in geothermal brines. According to the concentration of these ions in four different sources of brines (*SI Appendix*, Table S1), we evaluated the electrochemical performance of lithium extraction under the concentration ratios of 1:1 for the Li^+:Mg^{2+} and Li^+:Ca^{2+} systems, as well as 1:1 and 1:10 for Li^+:K^+ system. In the presence of a mixture of 0.01 M MgCl2 (Fig. 4*A*) and 0.01 M $CaCl_2$ (Fig. 4*B*) with 0.01 M LiCl, the cell voltages remained stable at around 1.0 V for above 150 min, achieving a high t_{Li+} of 94.7 ± 11.0% for $MgCl_2$ and 97.8 ± 2.0% for $CaCl_2$. Moreover, the cell voltages of 0.01 M KCl and 0.1 M KCl mixed with 0.01 M LiCl exhibited remarkable stability, almost overlapping in Fig. 4*C*. For the above

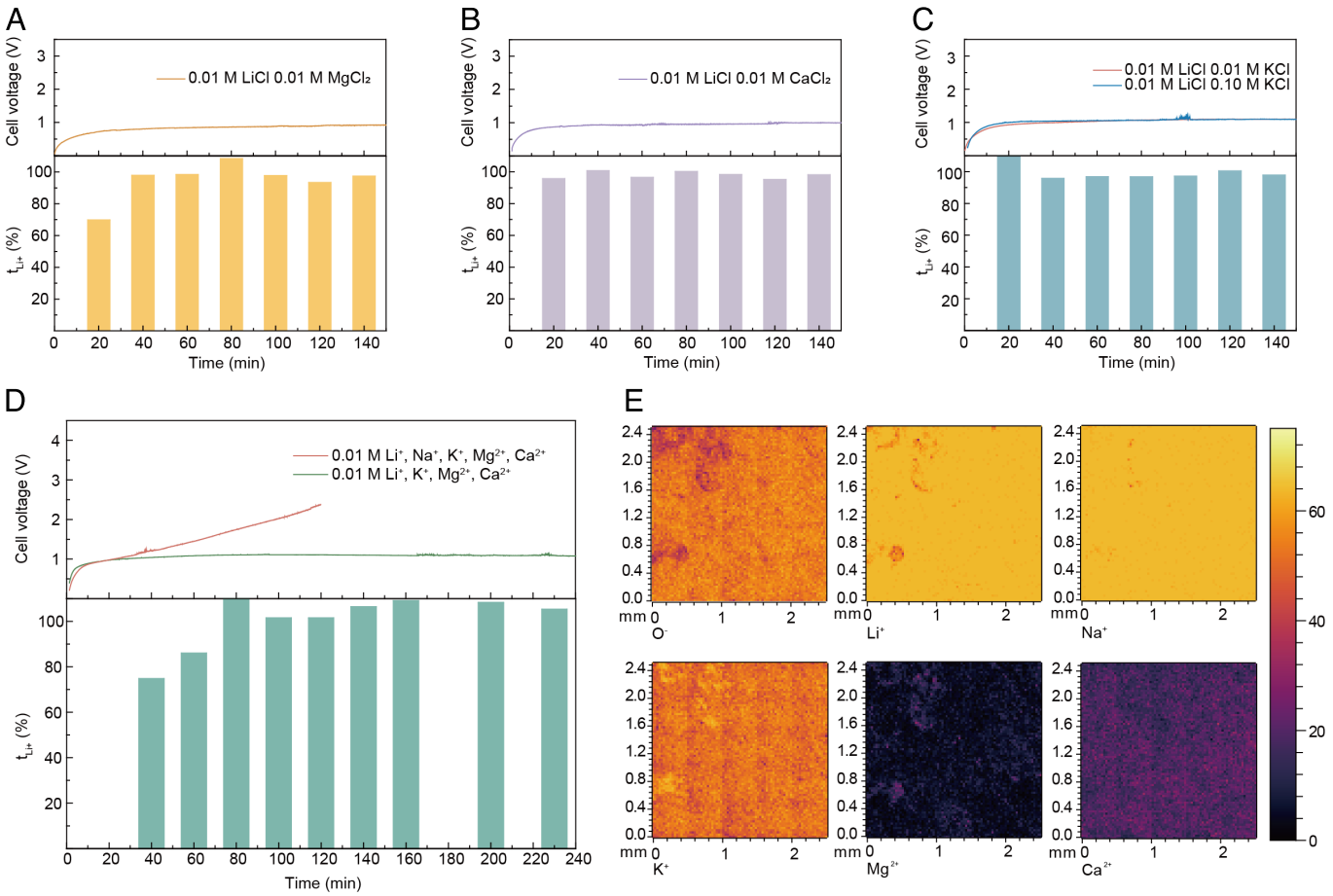

Fig. 4. Electrochemical performance and TOF-SIMS images of the LICGC membrane with $MgCl_2$, $CaCl_2$, and KCl brines. (*A*) Cell voltage (yellow curve) and t_{Li+} for lithium recovery from a simulated brine (0.01 M $MgCl_2$ and 0.01 M LiCl) under 0.1 mA (25 μA/cm2). (*B*) Cell voltage (purple curve) and t_{Li+} for lithium recovery from a simulated brine (0.01 M $CaCl_2$ and 0.01 M LiCl) under 0.1 mA (25 μA/cm2). (*C*) Cell voltage (blue curve) and t_{Li+} for lithium recovery from a simulated brine (0.10 M KCl and 0.01 M LiCl) under 0.1 mA (25 μA/cm2), and cell voltage (red curve) for lithium recovery from a simulated brine (0.01 M KCl and 0.01 M LiCl) under 0.1 mA (25 μA/cm2). (*D*) Cell voltage (blue curve) and t_{Li+} for lithium recovery from a simulated brine (0.01 M $MgCl_2$, $CaCl_2$, 0.01 M KCl, and 0.01 M LiCl) under 0.1 mA (25 μA/cm^2), and cell voltage (red curve) for lithium recovery from a simulated brine (0.01 M $MgCl_2$, $CaCl_2$, 0.01 M KCl, 0.01 M NaCl, and 0.01 M LiCl) under 0.1 mA (25 μA/cm2). (*E*) Normalized intensity of O^-, Li^+, Na^+, K^+, Mg^{2+}, and Ca^{2+} on the surface (facing the *Middle* layer) of the LICGC membrane.

three experiments, no peak of K^+, Mg^{2+}, or Ca^{2+} was observed in the catholyte using IC.

In the absence of Na^+ in the intermediate layer, a system comprising 0.01 M of Li^+, K^+, Mg^{2+}, and Ca^{2+} demonstrated stable operation for a duration of 240 min, as illustrated by the green curve in Fig. 4*D*. In contrast, the introduction of Na^+ into the system led to an increase in cell voltage, reaching approximately 2.5 V within 120 min (red curve in Fig. 4*D*). This outcome indicates that the presence of Na^+ uniquely impedes the transport of Li^+ ions. Subsequent TOF-SIMS analysis conducted on the LICGC membrane after the operation with 0.01 M Li^+, Na+, K^+, Mg^{2+}, and Ca^{2+} for 120 min (Fig. 4*E*) reveals that the signal intensity of Na on the membrane surface was nearly comparable to that of Li. The signal for K was lower, and the signals for Mg and Ca were markedly low. The TOF-SIMS results aligned with the electrochemical findings, emphasizing Na^+ as the ion most likely to undergo adsorption onto the surface of the LICGC membrane, thereby obstructing the transport pathway of Li^+. Conversely, the presence of K^+, Mg^{2+}, and Ca^{2+} did not adversely affect lithium extraction performance.

Conclusions

This study developed an electrochemical reactor featuring three chambers separated by two CEMs. By directing brine flow into the middle layer, the Cl^- concentration was reduced, mitigating the CER on the anode side. Additionally, the middle layer played a crucial role in buffering the H^+ concentration, resulting in a 2.1-fold improvement in t_{Li+} on the cathode side. The incorporation of a LICGC membrane to the three-chamber reactor enabled the direct and continuous production of LiOH, achieving an impressive t_{Li+} of 97.5% and a high Li^+ to Na^+, K^+, Mg^{2+}, and Ca^{2+} selectivity. Control experiments and TOF-SIMS analysis of the LICGC membrane surface were conducted to elucidate the ion transport behavior within the system. Our findings showed that Li^+ adsorption onto the LICGC membrane surface, particularly under higher applied currents, obstructed Li^+ transport through the membrane, leading to increased cell voltage. Conversely, the presence of K^+, Mg^{2+}, and Mg^{2+} did not adversely impact the transport of Li^+, as evidenced by stable cell voltages and the TOF-SIMS results. To enhance LICGC stability, surface coatings could be explored for future studies, and a pulse-reverse method may aid in recovering LICGC performance after fouling. Our research enhances the understanding of selective cation transport mechanisms on the interface of the LICGC, informs the design of advanced lithium-conducting and selective membranes, and sheds light on the development of more efficient and sustainable lithium extraction technologies.

Materials and Methods

Materials and Chemicals. Lithium chloride (LiCl, 99%, 793620-500 G), sodium chloride powder (NaCl, ≥99.5%, S7653-1 KG), Nafion-117 solution (527084-25 mL), Dowex 50W X8 (200 to 400 mesh, 44509-100 g) were purchased from Sigma Aldrich. Pt/C powder (20%-5 grams), hydrophobic gas diffusion layer carbon paper (GDL, Sigracet 28 BC), and Nafion-117 membranes were purchased from the Fuel Cell Store. IrO_2 electrode was purchased from the Dioxide Materials. The Lithium conductive ceramic membranes ($Li_{1+x+y}Al_xTi_{2-x}Si_yP_{3-y}O_{12}$, LICGC™ SP-01) are purchased from Ohara. Millipore water (18.2 M*Ohm*· cm) was used throughout all experiments.

Preparation of Pt/C Electrodes for HER Reaction. Typically, 40 mg active catalyst (Pt/C) and 80 μL of Nafion-117 binder solution were mixed with 4 mL of Isopropyl alcohol (Sigma-Aldrich). After sonication in ice water for 30 min, the obtained homogeneous ink was air-brushed onto a 5 × 5 cm^2 hydrophilic GDL electrode at 60 °C. Then the prepared electrode was further dried at room temperature before use.

Electrochemical Measurement. The cathode side was supplied with DI water for HER reaction. The water flow rate was controlled by a syringe pump at 0.5 mL/min. The flow rate at the outlet was calibrated using a measuring cylinder. In the middle chamber, the styrene-divinylbenzene sulfonated copolymer Dowex 50W X8 hydrogen form cation conductor was employed as the solid electrolyte (SE). The simulated brine flowed into the SE layer controlled by a syringe pump at 1.0 mL/min. All cell resistance was measured by potentiostatic electrochemical impedance spectroscopy, and all the cell voltages in our work were reported without any IR compensation. The transference number of a cation i^+ (t_{i+}) in the cathode is calculated using the following equation:

$$t_{i+} = \frac{C_{i+} \cdot F \cdot f}{j_{\text{total}}} \cdot 100\%, \quad [1]$$

where C_{i+} is the concentration of i^+ (mol/L), F is the Faraday constant (96,485 C mol^{-1}), f is the flow rate (L/s), and j_{total} is the total current (mA).

Li^+/Na^+ Selectivity Factor. The Li^+ and Na^+ concentration is measured using ion chromatography (IC, Shimadzu Corporation), calibrated using sodium and lithium standards purchased from Sigma Aldrich. The phosphate concentration is measured using inductively coupled plasma optical emission spectroscopy (ICP-OES), calibrated using phosphorus standard purchased from Sigma Aldrich. The Li^+/Na^+ selectivity ratio is calculated using the following equation:

$$Li^+/Na^+ selectivity = \frac{C_{Li}(out)}{C_{Na}(out)} \cdot \frac{C_{Na}(in)}{C_{Li}(in)}, \quad [2]$$

where C_{Li} (out) and C_{Na} (out) are the Li^+ and Na^+ concentrations in the cathode outflow, C_{Li} (in) and C_{Na}(in) are the Li^+ and Na^+ concentrations in the middle-layer inflow.

Chlorine Titration. The active chlorine produced in the anode side is quantified using the titration method with Sodium thiosulfate ($Na_2S_2O_3$). The active chlorine is first captured using the 5 mL 0.1 M KOH solution ($Cl_2 + 2KOH = KClO + KCl + H_2$). The pH was then adjusted back to acidic using 1 mL 0.5 M H_2SO_4. 1 mL 20% KI was then added to the solution ($KCl) + 2KI + 2H^+ = I_2 + 2K^+ + H_2O$), and the solution was kept in the dark for 5 min. Finally, 0.01 M Na2S2O3 solution was used for the titration ($2Na_2S_2O_3 + I_2 = Na_2S_4O_6 + 2NaI$), and the endpoint of the titration is indicated by starch.

TOF-SIMS Analysis. TOF-SIMS measurement was performed using a TOF-SIMS NCS instrument, which combines a TOF.SIMS5 instrument (ION-TOF GmbH, Münster, Germany) and an in situ scanning probe microscope (NanoScan, Switzerland) at Shared Equipment Authority from Rice University. A bunched 30 · keV Bi^{3+} ions (with a measured current of 0.15 pA) was used as the primary probe for analysis (scanned area 150 × 150 μm^2) with a raster of 128×128 pixels. A charge compensation with an electron flood gun has been applied during the analysis. An adjustment of the charge effects has been operated using appropriate surface potential and adapted extraction bias depending on the analysis area and the polarity. The cycle time was fixed to 100 μs (corresponding to m/z = 0 to 911 a.m.u mass range). The primary ion dose density has been limited to 1.1012 ions/cm^2 to preserve the analyzed surface. Depth profiling of the membrane was performed to map out the different samples to characterize the in-depth chemical distribution of the element ions of interest. The primary probe for depth profiling had a field of view of 150 × 150 μm^2, with a raster of 64 × 64 pixels and then the sputtering was performed

using Cs^+ ions at 2 keV with a typical current around 105 nA, raster area $500 \times 500\ \mu m^2$. The beams were operated in noninterlaced mode, alternating 1 analysis cycle and 5 sputtering cycles (corresponding to 7.5 s) followed by a pause of 3 s for the charge compensation with an electron flood gun. Again, an adjustment of the charge effects has been operated using a surface potential. During the depth profiling, the cycle time was fixed to 90 μs (corresponding to m/z = 0 to 738 a.m.u mass range). All of the data have been treated and extracted using SurfaceLab 7.3. Ion signals from spectra and from ion mappings have been normalized using the total ion signal to standardize the values and to help for the comparison between the different samples or the area.

Data, Materials, and Software Availability. All study data are included in the article and/or *SI Appendix*.

ACKNOWLEDGMENTS. This material is based upon work supported by the U.S. Department of Energy's Office of Energy Efficiency and Renewable Energy under Award DE-EE0010881. This work is also conducted in part using resources of the Shared Equipment Authority at Rice University. The authors appreciate proofreading support from Tracy Volz, George. R. Brown School of Engineering at Rice University.

Author affiliations: [a]Department of Chemical and Biomolecular Engineering, Rice University, Houston, TX 77005; [b]Secondary Ion Mass Spectrometry laboratory, Shared Equipment Authority, Rice University, Houston, TX 77005; [c]Department of Materials Science and NanoEngineering, Rice University, Houston, TX 77005; [d]Department of Chemistry, Rice University, Houston, TX 77005; and [e]Rice Advanced Material Institute, Rice University, Houston, TX 77005

Author contributions: Y.F., H.W., and S.L.B. designed research; Y.F., Y.P., S.H., Z.F., T.T., X.Z., C.Q., S.Z., F.C., P.Z., and Q.N. performed research; S.H., Z.F., T.T., X.Z., C.Q., S.Z., F.C., P.Z., and Q.N. contributed new reagents/analytic tools; Y.F., Z.F., T.T., H.W., and S.L.B. analyzed data; and Y.F., T.T., H.W., and S.L.B. wrote the paper.

Competing interest statement: Y.F., Z.F., H.W., and S.L.B. are inventors on a provisional United States patent application titled "Electrochemical Manufacturing of Lithium Hydroxide from Geothermal Brines in a Three-chamber Solid Electrolyte Reactor using a LICGC membrane" for the technology related to this work.

1. P. K. Choubey, M. S. Kim, R. R. Srivastava, J. C. Lee, J. Y. Lee, Advance review on the exploitation of the prominent energy-storage element: Lithium. Part I: From mineral and brine resources. *Miner. Eng.* **89**, 119–137 (2016).
2. P. K. Choubey, K. S. Chung, M. S. Kim, J. C. Lee, R. R. Srivastava, Advance review on the exploitation of the prominent energy-storage element Lithium. Part II: From sea water and spent lithium ion batteries (LIBs). *Miner. Eng.* **110**, 104–121 (2017).
3. V. Flexer, C. F. Baspineiro, C. I. Galli, Lithium recovery from brines: A vital raw material for green energies with a potential environmental impact in its mining and processing. *Sci. Total Environ.* **639**, 1188–1204 (2018).
4. G. Liu, Z. Zhao, A. Ghahreman, Novel approaches for lithium extraction from salt-lake brines: A review. *Hydrometallurgy* **187**, 81–100 (2019).
5. S. Yang, F. Zhang, H. Ding, P. He, H. Zhou, Lithium metal extraction from seawater. *Joule* **2**, 1648–1651 (2018).
6. C. Xu *et al*., Future material demand for automotive lithium-based batteries. *Commun. Mater.* **1**, 99 (2020).
7. P. Greim, A. A. Solomon, C. Breyer, Assessment of lithium criticality in the global energy transition and addressing policy gaps in transportation. *Nat. Commun.* **11**, 4570 (2020).
8. S. E. Kesler *et al*., Global lithium resources: Relative importance of pegmatite, brine and other deposits. *Ore Geol. Rev.* **48**, 55–69 (2012).
9. C. Grosjean, P. H. Miranda, M. Perrin, P. Poggi, Assessment of world lithium resources and consequences of their geographic distribution on the expected development of the electric vehicle industry. *Renew. Sust. Energy Rev.* **16**, 1735–1744 (2012).
10. D. E. Garrett, *Handbook of Lithium and Natural Calcium Chloride* (Elsevier, 2004).
11. X. Liu, M. Zhong, X. Chen, Z. Zhao, Separating lithium and magnesium in brine by aluminum-based materials. *Hydrometallurgy* **176**, 73–77 (2018).
12. B. Swain, Recovery and recycling of lithium: A review. *Sep. Purif. Technol.* **172**, 388–403 (2017).
13. D. A. Boryta, T. F. Kullberg, A. M. Thurston, "Recovery of lithium compounds from brines." US Patent 6207126B1 (2001).
14. Q. H. Zhang, S. P. Li, S. Y. Sun, X. S. Yin, J. G. Yu, Lithium selective adsorption on low-dimensional titania nanoribbons. *Chem. Eng. Sci.* **65**, 165–168 (2010).
15. R. Chitrakar, Y. Makita, K. Ooi, A. Sonoda, Synthesis of iron-doped manganese oxides with an ion-sieve property: Lithium adsorption from bolivian brine. *Ind. Eng. Chem. Res.* **53**, 3682–3688 (2014).
16. X. Xu *et al*., Extraction of lithium with functionalized lithium ion-sieves. *Prog. Mater. Sci.* **84**, 276–313 (2016).
17. C. Shi *et al*., Solvent extraction of lithium from aqueous solution using non-fluorinated functionalized ionic liquids as extraction agents. *Sep. Purif. Technol.* **172**, 473–479 (2017).
18. B. Swain, Separation and purification of lithium by solvent extraction and supported liquid membrane, analysis of their mechanism: A review: Separation and purification of lithium. *J. Chem. Technol. Biotechnol.* **91**, 2549–2562 (2016).
19. A. Campione *et al*., Electrodialysis for water desalination: A critical assessment of recent developments on process fundamentals, models and applications. *Desalination* **434**, 121–160 (2018).
20. Q. B. Chen *et al*., Development of recovering lithium from brines by selective-electrodialysis: Effect of coexisting cations on the migration of lithium. *J. Memb. Sci.* **548**, 408–420 (2018).
21. T. Hoshino, Innovative lithium recovery technique from seawater by using world-first dialysis with a lithium ionic superconductor. *Desalination* **359**, 59–63 (2015).
22. G. Liu, Z. Zhao, L. He, Highly selective lithium recovery from high Mg/Li ratio brines. *Desalination* **474**, 114185 (2020).
23. J. Xiao, F. Shi, T. Glossmann, C. Burnett, Z. Liu, From laboratory innovations to materials manufacturing for lithium-based batteries. *Nat. Energy* **8**, 329–339 (2023).
24. C. Liu *et al*., Lithium extraction from seawater through pulsed electrochemical intercalation. *Joule* **4**, 1459–1469 (2020).
25. G. T. Hill, F. Shi, H. Zhou, Y. Han, C. Liu, Layer spacing gradient (NaLi)1-xCoO2 for electrochemical Li extraction. *Matter* **4**, 1611–1624 (2021).
26. F. La Mantia, M. Pasta, H. D. Deshazer, B. E. Logan, Y. Cui, Batteries for efficient energy extraction from a water salinity difference. *Nano Lett.* **11**, 1810–1813 (2011).
27. M. S. Palagonia, D. Brogioli, F. La Mantia, Lithium recovery from diluted brine by means of electrochemical ion exchange in a flow-through-electrodes cell. *Desalination* **475**, 114192 (2020).
28. Y. Sun, Y. Wang, Y. Liu, X. Xiang, Highly efficient lithium extraction from brine with a high sodium content by adsorption-coupled electrochemical technology. *ACS Sust. Chem. Eng.* **9**, 11022–11031 (2021).
29. C. Xia *et al*., Continuous production of pure liquid fuel solutions via electrocatalytic CO_2 reduction using solid-electrolyte devices. *Nat. Energy* **4**, 776–785 (2019).
30. C. Xia, Y. Xia, P. Zhu, L. Fan, H. Wang, Direct electrosynthesis of pure aqueous H_2O_2 solutions up to 20% by weight using a solid electrolyte. *Science* **366**, 226–231 (2019).
31. P. Zhu *et al*., Continuous carbon capture in an electrochemical solid-electrolyte reactor. *Nature* **618**, 959–966 (2023).
32. X. Li *et al*., Membrane-based technologies for lithium recovery from water lithium resources: A review. *J. Memb. Sci.* **591**, 117317 (2019).
33. L. Gong, W. Ouyang, Z. Li, J. Han, Direct numerical simulation of continuous lithium extraction from high Mg2+/Li+ ratio brines using microfluidic channels with ion concentration polarization. *J. Memb. Sci.* **556**, 34–41 (2018).
34. A. Razmjou *et al*., Lithium ion-selective membrane with 2D subnanometer channels. *Water Res.* **159**, 313–323 (2019).
35. T. Hoshino, Preliminary studies of lithium recovery technology from seawater by electrodialysis using ionic liquid membrane. *Desalination* **317**, 11–16 (2013).
36. Y. Guo, Y. Ying, Y. Mao, X. Peng, B. Chen, Polystyrene sulfonate threaded through a metal-organic framework membrane for fast and selective lithium-ion separation. *Angew Chem. Int. Ed. Engl.* **55**, 15120–15124 (2016).
37. H. Zhang *et al*., Ultrafast selective transport of alkali metal ions in metal organic frameworks with subnanometer pores. *Sci. Adv.* **4**, eaaq0066 (2018).
38. C. Cai *et al*., Promising transport and high-selective separation of Li(I) from Na(I) and K(I) by a functional polymer inclusion membrane (PIM) system. *J. Membr. Sci.* **579**, 1–10 (2019).
39. S. J. Warnock *et al*., Engineering Li/Na selectivity in 12-Crown-4-functionalized polymer membranes. *Proc. Natl. Acad. Sci. U.S.A.* **118**, e2022197118 (2021).
40. W. Zhao, J. Yi, P. He, H. Zhou, Solid-state electrolytes for lithium-ion batteries: Fundamentals, challenges and perspectives. *Electrochem. Energy Rev.* **2**, 574–605 (2019).
41. B. Zhang *et al*., Mechanisms and properties of ion-transport in inorganic solid electrolytes. *Energy Storage Mater.* **10**, 139–159 (2018).
42. S. P. Ong *et al*., Phase stability, electrochemical stability and ionic conductivity of the Li10 ± 1MP2X12 (M = Ge, Si, Sn, Al or P, and X = O, S or Se) family of superionic conductors. *Energy Environ. Sci.* **6**, 148–156 (2013).
43. C. Yang, K. Fu, Y. Zhang, E. Hitz, L. Hu, Protected lithium-metal anodes in batteries: From liquid to solid. *Adv Mater.* **29**, 1701169 (2017).
44. Y. Wang, H. Zhou, A lithium-air battery with a potential to continuously reduce O_2 from air for delivering energy. *J. Power Sources* **195**, 358–361 (2010).
45. X. Wang, Y. Hou, Y. Zhu, Y. Wu, R. Holze, An aqueous rechargeable lithium battery using coated Li metal as anode. *Sci. Rep.* **3**, 1401 (2013).
46. T. Ounissi, L. Dammak, C. Larchet, J. F. Fauvarque, E. Selmane Bel Hadj Hmida, Novel lithium selective composite membranes: synthesis, characterization and validation tests in dialysis. *J. Mater. Sci.* **55**, 16111–16128 (2020).
47. J. Xu *et al*., A green and sustainable strategy toward lithium resources recycling from spent batteries. *Sci. Adv.* **8**, eabq7948 (2022).
48. Y. Wang, P. He, H. Zhou, A novel direct borohydride fuel cell using an acid-alkaline hybrid electrolyte. *Energy Environ. Sci.* **3**, 1515–1518 (2010).